

Heterogeneity can markedly increase final outbreak size in the SIR model of epidemics

Alexander Leibenzon  and Michael Assaf 

Racah Institute of Physics, Hebrew University of Jerusalem, Jerusalem 91904, Israel

 (Received 1 March 2023; revised 13 August 2023; accepted 14 December 2023; published 16 January 2024)

We study the susceptible-infected-recovered (SIR) model of epidemics on positively correlated heterogeneous networks with population variability, and explore the dependence of the final outbreak size on the network heterogeneity strength and basic reproduction number R_0 —the ratio between the infection and recovery rates per individual. We reveal a critical value R_0^c , above which the maximal outbreak size is obtained at zero heterogeneity, but below which the maximum is obtained at finite heterogeneity strength. This second-order phase transition, universal for all network distributions with finite standardized moments, indicates that network heterogeneity can greatly increase the final outbreak size. We also show that this effect can be enhanced by adding population heterogeneity, in the form of varying interindividual susceptibility and infectiousness. Our results provide key insight as to the predictability of the well-mixed SIR model for the final outbreak size, in realistic scenarios.

DOI: [10.1103/PhysRevResearch.6.L012010](https://doi.org/10.1103/PhysRevResearch.6.L012010)

Introduction. The SIR (susceptible-infected-recovered) model [1–3] has been a topic of great interest during the past decades [4], and is one of the most conceptually basic, yet powerful, models that describes the spread of an infectious disease. The model includes three population classes: susceptible (S), infected (I), and recovered (R). A contact between S and I individuals can give rise to the infection of S . Conversely, an infected individual can recover and move to the R class. Remarkably, this simple model provides an adequate description to a wide variety of infectious diseases including COVID-19 pandemic [5].

Many works dealing with the SIR model assume a well-mixed (or homogeneous) topology [2,3,6–8]. While this assumption is valid in some limits, in realistic scenarios one has to account for each individual’s connectivity and deal instead with a *population network*. Indeed, in the past 20 years various authors studied the SIR model and epidemic spreading on heterogeneous random networks, where different individuals have varying connectivity [6,9–14]. In most of these works a mean-field approach is taken; i.e., noise is neglected. Other works have gone beyond mean field, by including demographic noise in the well-mixed SIR model. This allows, e.g., studying the final outbreak size *distribution* [15–21]. Nevertheless, even in the absence of noise, the direct influence of the network topology on the final outbreak size has not been investigated. Importantly, this may be key for predicting the outcome of such a disease, as we show that the well-mixed (fully-connected) setting does not necessarily provide an upper bound for the final outbreak size.

Here we discover a novel second-order phase transition in the maximal outbreak size as a function of the network heterogeneity. Intuitively, as the network heterogeneity is increased,

the final outbreak size should decrease, and thus, the outbreak size is expected to be maximal at zero heterogeneity. This is indeed the case for large values of the basic reproduction number R_0 . For a well-mixed setting, $R_0 = \beta/\gamma$; i.e., the ratio between the infection rate β and recovery rate γ per individual. However, it turns out that there exists a critical value of R_0 , which we denote by R_0^c , below which the maximal outbreak size is obtained at *nonzero* heterogeneity. Furthermore, as R_0 is decreased below R_0^c , the magnitude of heterogeneity which maximizes the final outbreak size is increased. Interestingly, by introducing population heterogeneity in the form of varying susceptibility and/or infectiousness across individuals [22–28], this effect is enhanced, and the phase transition moves to increasingly larger values of R_0^c . In contrast, we find that the value of R_0^c decreases as the degree-degree correlation between neighboring nodes increases. Finally, we show that this phase transition is universal, namely R_0^c is independent on the network topology, as long as the degree distribution has finite standardized moments. Our results provide key insight as to the limits of applicability of the simplified well-mixed SIR model to real-life heterogeneous networks with respect to the final outbreak size.

SIR model on networks. In the SIR model the total population is conserved: $S + I + R = N$. Here, N is the network size—the number of agents spreading the infection. Using the fractions of susceptibles $S = S/N$, infected $I = I/N$, and recovered $R = R/N$, denoting $R_0 = \beta/\gamma$, rescaling time $t \rightarrow \gamma t$, and assuming a well-mixed setting, in the limit of $N \gg 1$ the dynamics read

$$\dot{S} = -R_0 I S, \quad \dot{I} = R_0 I S - I, \quad \dot{R} = I. \quad (1)$$

Notably, Eq. (1) ignores demographic noise, whose relative magnitude scales, in general, as $N^{-1/2} \ll 1$ [29,30]. Moreover, in deriving Eq. (1) we used a fully-connected network, where each individual interacts with all others.

We now account for network heterogeneity by considering a population network, where each node represents an individual who can be either susceptible, infected or recovered, and

Published by the American Physical Society under the terms of the [Creative Commons Attribution 4.0 International license](https://creativecommons.org/licenses/by/4.0/). Further distribution of this work must maintain attribution to the author(s) and the published article’s title, journal citation, and DOI.

edges between nodes represent interactions between them. We follow the formalism developed by Miller [9] and define $p(k)$ as the network degree distribution. Namely, $p(k)$ is the probability for a node to have k neighbors. We also assume that the network has positive degree-degree correlations [31], see below. Henceforth, we assume that the reproduction number R_0 is above the epidemic threshold, see Appendix A.

Let us denote $\theta(t)$ as the probability that a random edge has not transmitted an infectious contact up to a time t . This definition is equivalent to the probability that a node of degree 1 is still susceptible at time t [10]. Thus, the probability of an individual node with k neighbors to remain susceptible at time t is given by θ^k . As a result, the fraction of susceptibles at time t is given by

$$S(t) = \sum_{k=0}^{\infty} p(k)\theta(t, \sigma)^k \equiv \psi(\theta, \sigma). \quad (2)$$

Here, $\sigma^2 = \sum_k k^2 p(k) - k_0^2$ is the degree distribution's variance, and $k_0 = \sum_k k p(k)$ is its mean. Also, $\psi(\theta, \sigma)$ is the probability generating function of $p(k)$; its derivatives with respect to θ at $\theta = 0$ provide the distribution $p(k)$, while the derivatives at $\theta = 1$ provide the distribution's moments, e.g., $k_0 = \partial_\theta \psi|_{\theta=1}$. Though ψ depends on the entire distribution $p(k)$, an explicit σ -dependence in ψ is included, as we focus on how the final outbreak size depends on σ .

We now derive the governing equation for $\theta(t, \sigma)$ in order to obtain the final susceptible fraction, $S_\infty = \psi(t \rightarrow \infty)$, and the final outbreak fraction $R_\infty = 1 - S_\infty$. Below we set $\gamma = 1$, such that time is measured in units of γ^{-1} , and rescale $\beta \rightarrow \beta/k_0$, such that β now denotes the average rate of infection transmission through an edge. The average infection rate per individual is thus $k_0\beta$ and the basic reproduction number takes the form $R_0 = k_0\beta/\gamma$ in order to be consistent with the well-mixed case. Defining an auxiliary variable $\phi(t)$ as the probability that a node v is infectious but has not transmitted the disease to its neighbor u , ϕ denotes the fraction of all $v - u$ edges in the network where v is infected but has not (yet) directly infected u . Thus, $\dot{\theta} = -\beta\phi$ [9].

The dynamics of $\phi(t)$ satisfies $\dot{\phi} = -(\beta + 1)\phi - \dot{h}$. Here, ϕ decreases when the neighbor u is infected from v at rate $\beta\phi$, or when node v is recovered at a rate of $\gamma\phi = \phi$. On the other hand, ϕ increases when a susceptible node v becomes infected. Here, $h(t)$ is the probability that v remains susceptible, and thus, $-\dot{h}(t)$ is the rate at which v becomes infected from any of its neighbors except u . Accounting for positive degree-degree correlations, the probability that a neighbor of a degree- k' node has degree k , i.e., the two-point degree correlation function, satisfies $p(k|k') = (1 - \alpha)k p(k)/k_0 + \alpha \delta_{k,k'}$ [31], where $\alpha > 0$ measures the correlation strength [32]. Therefore, $h(t) = \sum_{k'=0}^{\infty} \sum_{k=0}^{\infty} p(k|k') p(k') \theta^{k-1} = (1 - \alpha)k_0^{-1} \partial_\theta \psi(\theta, \sigma) + \alpha \theta^{-1} \psi(\theta, \sigma)$. This derivation yields $\dot{\phi} = (1 + 1/\beta)\dot{\theta} - \dot{h}$, which can be integrated over time, using the fact that $\phi(0) = 0$, $\theta(0) \simeq 1$ and $h(0) = 1$. As a result,

$$\dot{\theta} = 1 - \left(1 + \frac{R_0}{k_0}\right)\theta + \frac{R_0}{k_0} \left(\frac{1 - \alpha}{k_0} \partial_\theta \psi + \frac{\alpha}{\theta} \psi\right). \quad (3)$$

This is a first-order nonlinear differential equation, which strongly depends on the network topology and degree-degree correlations. While its time-dependent solution can be found

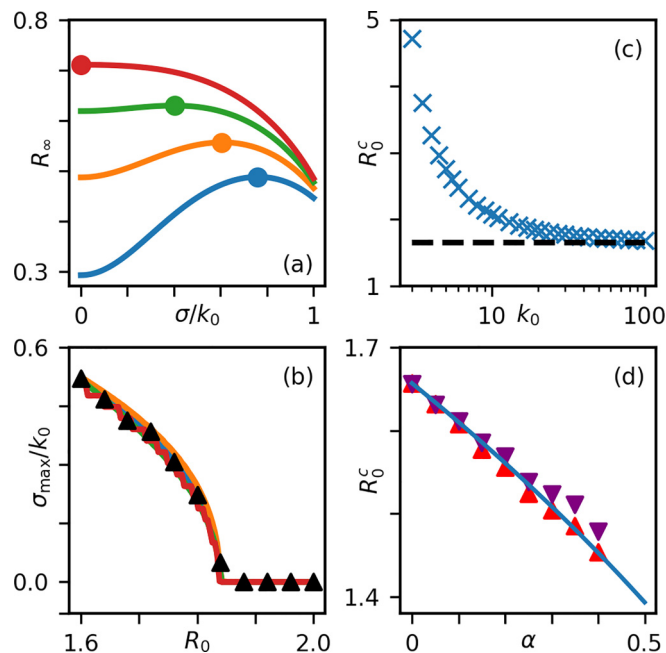


FIG. 1. (a) A numerical solution of R_∞ versus the network's COV σ/k_0 for a bimodal network, see text: blue, orange, green, and red lines represent $R_0 = 1.3, 1.5, 1.7, 1.9$ respectively. (b) σ_{\max}/k_0 , which maximizes R_∞ versus R_0 : blue, orange, green, and red lines, respectively represent bimodal, symmetric beta, gamma, and uniform distributions, while black triangles are simulation results for a bimodal network. Here $R_0^c \simeq 1.84$. (c) R_0^c versus k_0 ; dashed line is the asymptotic value of $(3/2)\ln 3$. (d) R_0^c versus α ; solution of Eq. (5) (solid line) is compared with simulations of bimodal (upper triangles) and gamma (lower triangles) distributions. In panels (a)–(c) $N = 10^4$ and in (a)–(b) $k_0 = 20$, while in (d) $N = 10^5$ and $k_0 = 100$.

numerically, we study its steady-state solution $\theta_\infty \equiv \theta(t \rightarrow \infty)$. Putting $\dot{\theta} = 0$ in Eq. (3) we find

$$\theta_\infty(\sigma) = \frac{R_0}{R_0 + k_0} \left[\frac{1 - \alpha}{k_0} \partial_\theta \psi + \frac{\alpha}{\theta_\infty} \psi + \frac{k_0}{R_0} \right] \Big|_{\theta=\theta_\infty}. \quad (4)$$

Note that, for $\alpha = 0$ the results of Ref. [9] are recovered.

Maximal outbreak size. Equation (4) can be numerically solved for various network topologies $p(k)$, having mean k_0 and variance σ^2 . An example for the dependence of R_∞ on σ , for various values of R_0 , can be seen in Fig. 1(a) where we have used a bimodal network, with $p(k) = 1/2(\delta_{k,k_0-\sigma} + \delta_{k,k_0+\sigma})$. Remarkably, as R_0 is lowered below some threshold R_0^c , the maximum of R_∞ shifts from $\sigma = 0$ to $\sigma > 0$. That is, while for $R_0 > R_0^c$, the final outbreak size is maximized when the network is homogeneous, for $R_0 < R_0^c$ the maximum is obtained at finite heterogeneity. This is a surprising result. Indeed, as σ is increased, the final outbreak size should decrease, as nodes with very high degree become more abundant. Due to their high degree, these nodes get infected (and recovered) much quicker than low-degree nodes, which causes a more rapid decrease in the effective infection rate per individual, and correspondingly, in the final outbreak size, compared to the homogeneous case. Yet, we show below that this reasoning breaks down when $R_0 < R_0^c$.

We have studied the dependence of the threshold R_0^c on the network's degree distribution. In Fig. 1(b), we plot the value of the coefficient of variation (COV) σ_{\max}/k_0 , which maximizes the final outbreak size, for bimodal, symmetric beta, gamma and uniform distributions, versus R_0 , for $k_0 = 20$ and $\alpha = 0$. The fact that all curves in Fig. 1(b) collapse indicates that R_0^c is independent on the particular network details, see below.

To find R_0^c we realize that at the threshold $R_0 = R_0^c$, the maximum of R_∞ is obtained exactly at $\sigma = 0$, namely $dR_\infty/d\sigma|_{\sigma=0} = 0$. Above R_0^c this derivative is negative, whereas below R_0^c the maximum is obtained for $\sigma > 0$, see Fig. 1(a). Differentiating $R_\infty = 1 - \psi(\theta_\infty, \sigma)$ with respect to σ , using Eqs. (2) and (4), and demanding that the derivative $dR_\infty/d\sigma$ be zero at $\sigma = 0$, we arrive at

$$k_0 + \frac{k_0^2}{R_0^c} = \left[(1 - \alpha) \left(\partial_{\theta\theta} \psi - \frac{\partial_\theta \psi \partial_{\sigma\theta} \psi}{\partial_\sigma \psi} \right) - \frac{\alpha k_0}{\theta^2} \psi \right] \Big|_{\substack{\theta = \theta_\infty \\ \sigma = 0}}. \quad (5)$$

This is an exact algebraic equation, whose solution provides R_0^c . In general it can be solved numerically, whereas analytical progress can be made for $k_0 \gg 1$. Here we seek for the solution perturbatively by assuming $\theta_\infty = 1 - \epsilon$ with $\epsilon = \mathcal{O}(k_0^{-1}) \ll 1$ (to be verified *a posteriori*).

First, we establish a connection between ϵ and R_0^c by plugging $\theta_\infty = 1 - \epsilon$ into Eq. (4), and putting $\sigma = 0$, i.e., using a homogeneous distribution $p(k) = \delta_{k,k_0}$. Keeping leading order terms we arrive at $\epsilon k_0 \simeq R_0^c [1 - \exp(-\epsilon k_0)]$, the solution of which is given via the Lambert W -function

$$\epsilon = k_0^{-1} \{ R_0^c + W_0[-R_0^c \exp(-R_0^c)] \}. \quad (6)$$

Going back to Eq. (5), for $k_0 \gg 1$, $\psi(\theta_\infty) = \theta_\infty^{k_0}$ can be approximated as $\theta_\infty^{k_0} = \exp(-\epsilon k)$, with $\mathcal{O}(k\epsilon^2) \ll 1$ corrections in the exponent. Thus, the two terms $\partial_\theta \psi(\theta, \sigma)$ and $\partial_{\theta\theta} \psi(\theta, \sigma)$ evaluated at $\theta = \theta_\infty$ and $\sigma = 0$, read

$$\partial_{\theta\theta} \psi = e^{-\epsilon k_0} k_0^2 [1 + \mathcal{O}(\epsilon)], \quad \partial_\theta \psi = e^{-\epsilon k_0} k_0 [1 + \mathcal{O}(\epsilon)]. \quad (7)$$

Notably, the terms involving derivatives with respect to σ in Eq. (5) are more involved as one has to use the definition of ψ from Eq. (2). To proceed, we write

$$\frac{\partial_{\sigma\theta} \psi(\theta, \sigma)}{\partial_\sigma \psi(\theta, \sigma)} = k_0 - \partial_\epsilon \ln \partial_\sigma \{ e^{-\epsilon(k-k_0)} \} + \mathcal{O}(1), \quad (8)$$

where this expression has to be evaluated at $\theta = \theta_\infty$ and $\sigma = 0$. Here, we added k_0 , and subtracted k_0 by subtracting k_0 from k in the exponent. The term in the brackets is (up to a minus sign) the generating function of the central moments (around the mean) $\{\mu_n\}_{n=0}^\infty$. Taylor-expanding in powers of $\epsilon(k - k_0)$, we find $\langle e^{-\epsilon(k-k_0)} \rangle = \sum_k p(k) - \epsilon \sum_k p(k)(k - k_0) + (\epsilon^2/2) \sum_k p(k)(k - k_0)^2 - (\epsilon^3/6) \sum_k p(k)(k - k_0)^3 + \dots = 1 + (\epsilon^2/2)\sigma^2 - (\epsilon^3/6)\mu_3 + \dots$, where $\mu_1 = 0$ and $\mu_2 = \sigma^2$. For $p(k)$ with finite standardized moments $\tilde{\mu}_n$, one can show that $\mu_n = \sigma^n \tilde{\mu}_n$. As a result, plugging this series back into Eq. (8), all terms with powers of σ greater than 2 vanish, since we set $\sigma = 0$ after the differentiation, and one finally obtains $\partial_{\sigma\theta} \psi(\theta, \sigma)/\partial_\sigma \psi(\theta, \sigma) = k_0 - 2/\epsilon + \mathcal{O}(1)$. Plugging this along with Eq. (7) into Eq. (5), and using Eq. (6), in the leading order of $k_0 \gg 1$ the critical R_0^c is found

to be

$$R_0^c = [(3 - 2\alpha)/(2 - 2\alpha)] \ln(3 - 2\alpha). \quad (9)$$

For uncorrelated networks $\alpha = 0$, we find $R_0^c = (3/2) \ln 3 \simeq 1.648$. Plugging R_0^c into Eq. (6) verifies *a posteriori* that $\epsilon = \mathcal{O}(k_0^{-1})$. In Fig. 1(c) we have numerically checked that as k_0 is increased, R_0^c approaches Eq. (9) [33]. Notably, the numerical value of $R_0^c \simeq 1.84$, obtained in Fig. 1(b) for $k_0 = 20$, slightly deviates from Eq. (9).

To verify our results we ran Gillespie simulations [34] on correlated, bimodal-, and gamma-distributed networks. In Fig. 1(b) the network size was $N = 10^4$, with $k_0 = 20$ and $\alpha = 0$, while in Fig. 1(d) we took $N = 10^5$, $k_0 = 100$, and varied the value of α . The simulations were done using a modified version of the configuration model [35], see details in Appendix B. In Figs. 1(b) and 1(d) our analytical prediction, Eq. (9), agrees well with simulations for $\alpha \geq 0$. While we focus on $\alpha \geq 0$ indicative of social networks [36], we checked that for $\alpha < 0$, R_0^c grows as expected.

What is the reason for the second-order phase transition observed in Fig. 1(b)? The total outbreak fraction satisfies $R_\infty = \int_0^\infty I(t) dt$. Several examples of epidemic waves for various COV values are shown in Fig. 2(a). We propose to approximate R_∞ as $R_\infty \simeq c I_{\max} \Delta t$, where I_{\max} is the maximal value of I (that defines herd immunity), and Δt is the typical wave's duration: the time interval during which I is greater than a fraction f (yet to be found) of I_{\max} , while c is a constant. For the distributions we have studied, f and c were found to satisfy $f \approx 0.27$ and $c \approx 0.785$ for a wide range of $R_0 = \mathcal{O}(1)$ and σ values. In Fig. 2(b) the approximate and exact solutions for R_∞ agree well, for bimodal networks [37].

To explain the appearance of a phase transition at R_0^c , we denote by \tilde{I}_{\max} (and similarly for $\tilde{\Delta t}$) the ratio of I_{\max} at given σ and its value at $\sigma = 0$, see Figs. 2(c)–2(d), such that $\tilde{R}_\infty = \tilde{I}_{\max} \tilde{\Delta t}$. Thus, we have $\tilde{R}'_\infty(\sigma)/\tilde{R}_\infty(\sigma) = \tilde{I}'_{\max}(\sigma)/\tilde{I}_{\max}(\sigma) + \tilde{\Delta t}'(\sigma)/\tilde{\Delta t}(\sigma)$. At $R_0 > R_0^c$ we see from Fig. 2(e) that $\tilde{R}'_\infty(\sigma)/\tilde{R}_\infty(\sigma)$ is negative for any σ . Yet, as R_0 goes below R_0^c a nonmonotone regime appears, which gives rise to a maximum in R_∞ at $\sigma > 0$.

This can be understood as follows. As the network heterogeneity strength σ is increased, there are more very high degree nodes (hubs), which get infected first due to their high degree, and infect the entire network rapidly. This rapid epidemic spread causes I to surge, but also causes the epidemic's duration Δt to decrease. For low infection rates $R_0 < R_0^c$, increasing σ initially causes the increase of R_∞ as the increase of I_{\max} cannot be balanced by the decrease of Δt , see Figs. 2(c)–2(e). Notably, as σ exceeds σ_{\max} the dynamics of the hubs is so rapid such that low-degree nodes are hardly infected, and thus, R_∞ starts to decrease. This effect is further discussed in Appendix C, and can be seen in Fig. 4. Exactly at the onset of decrease of R_∞ , i.e., at $\sigma = \sigma_{\max}$, the disease spread rate is optimal such that the total fraction of infected nodes R_∞ is maximized. Interestingly, increasing R_0 has a similar effect to increasing σ ; when R_0 grows, the increase of σ is no longer needed to increase the disease spread rate. Thus, if σ is also increased, one exceeds the optimal disease spread rate which yields a decline in R_∞ . Therefore, if at $R_0 < R_0^c$ the maximum of R_∞ is obtained at $\sigma = \sigma_{\max} > 0$,

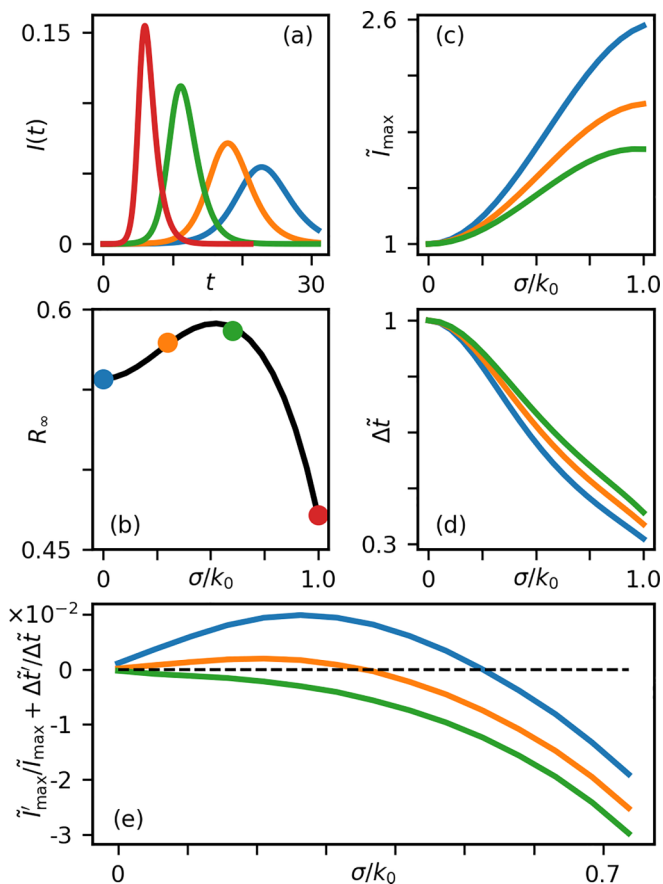


FIG. 2. (a) Infected fraction $I(t)$ versus time, for $R_0 = 1.6$. Blue, orange, green and red lines represent COVs $\sigma/k_0 = 0, 0.3, 0.6, 1$, respectively. (b) Line shows the approximation for the final outbreak fraction $cI_{\max} \Delta t$ versus the COV, for the same network as in (a). Dots represent numerical integration over $I(t)$ from (a). Panels (c), (d), and (e), respectively, show \tilde{I}_{\max} , $\Delta \tilde{t}$, and $\tilde{R}'_{\infty}/\tilde{R}_{\infty} = I'_{\max}/I_{\max} + \Delta t'/\Delta t$ versus the COV, where prime denotes differentiation with respect to σ . In all panels we use a bimodal distribution with $k_0 = 20$ and $\alpha = 0$, and in (c)–(e) blue, orange, and green lines represent $R_0 = 1.65, 1.8, 1.95$, respectively (here $R_0 = 1.95$ is above R_0^c).

as R_0 is increased, σ_{\max} shifts towards zero, as increasing R_0 is complementary to increasing σ .

Population heterogeneity. We now add variability across the population (population heterogeneity) and study its effect on the phase transition, by using the formalism of Ref. [27] and modulating the infection rate β by the mean population's susceptibility \bar{x} , such that $R_0 \rightarrow \bar{x}R_0$. While for homogeneous populations $\bar{x}(t) = 1$, for heterogeneous populations, \bar{x} decays in time, as the highly susceptible individuals get infected and recover relatively quickly, thereby decreasing \bar{x} . In the well-mixed case, denoting by $s(x, t)$ the fraction of susceptibles having infection rate between x to $x + dx$, the total fraction of susceptibles is $S(t) = \int_0^{\infty} s(x, t) dx$. Thus, $s(x, t)$ satisfies $\partial_t s = -R_0 x s I$, and the mean susceptibility becomes [27]

$$\bar{x}(t) = S(t)^{-1} \int_0^{\infty} x s(x, t) dx. \quad (10)$$

To find $\bar{x}(t)$, a new time scale $\tau = R_0 I$ is defined, measuring the epidemic spreading. Thus, $d\tau/dt = R_0 I$, such that

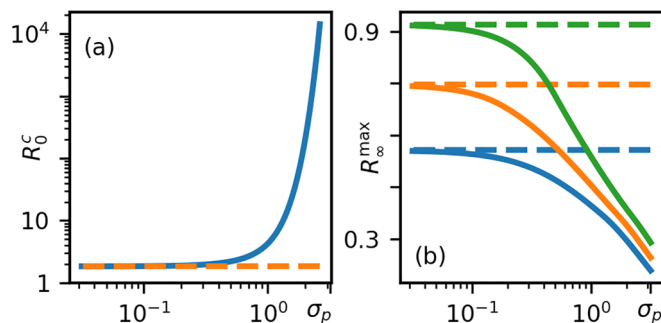


FIG. 3. (a) Critical basic reproduction number R_0^c versus population heterogeneity strength σ_p . Dashed line is $R_0^c \approx 1.84$, the asymptotic value of R_0^c at $\sigma_p \rightarrow 0$. (b) Maximal outbreak size R_{∞}^{\max} versus σ_p , for $R_0 = 1.5, 2, 3$ (blue, orange, and green lines, respectively). Dashed lines are the asymptotic values for $\sigma_p \rightarrow 0$. In both panels $k_0 = 20$ and $N = 10^4$.

$\partial_{\tau} s = -xs$, which yields $s(x, \tau) = s_0(x) \exp(-\tau x)$. We incorporate population heterogeneity by taking a gamma-distributed initial susceptibility $s_0(x) \sim x^{-1+a} e^{-ax}$, with average 1 and standard deviation $\sigma_p = a^{-1/2}$ [38]. With this distribution, \bar{x} given by Eq. (10) decays in time as $\bar{x} = (1 + \tau \sigma_p^2)^{-1}$ [27].

To combine network and population heterogeneity, we introduce the dynamical infection rate $\beta(t) = \bar{x}\beta = \bar{x}R_0/k_0$ with \bar{x} given by Eq. (10). For heterogeneous networks, θ and ϕ are connected via $\theta = -\beta\phi$. Using the equation for ϕ defined above Eq. (3), putting $\beta \rightarrow \bar{x}(t)\beta$, and differentiating θ with respect to time, we arrive at

$$\ddot{\theta} = \dot{\theta} \left\{ \frac{\dot{\bar{x}}}{\bar{x}} + \bar{x} \frac{R_0}{k_0} \left[(1-\alpha) \frac{\partial_{\theta\theta} \psi}{k_0} - \alpha \left(\frac{\psi}{\theta^2} - \frac{\partial_{\theta} \psi}{\theta} \right) - 1 \right] - 1 \right\}, \quad (11)$$

where we have assumed a correlation strength α . The validity of Eq. (11) can be checked in two limits. In the limit of a homogeneous population, $\bar{x} \rightarrow 1$ and Eq. (3) is restored upon integration over time. In the well-mixed limit, $k_0 \simeq N \gg 1$, $\theta = 1 - \mathcal{O}(k_0^{-1})$; here a proportion of $\mathcal{O}(I/k_0)$ of edges emanating from each node transmits the infection from a still infected node [9]. Thus, $\phi = 1 - \mathcal{O}(I/k_0)$, $\psi'(\theta) = k_0 S/\theta$, and $\dot{S} = -\psi'(\theta)\dot{\theta} = -R_0 \bar{x} S I + \mathcal{O}(SI/k_0)$, which coincides in the leading order with the well-mixed SIR model under population heterogeneity [27,28].

To find R_0^c under both population and network heterogeneity, we numerically compute the steady-state solution of Eq. (11), which allows finding $R_{\infty}(R_0)$. Here, as \bar{x} decreases over time, the effective disease spread rate $\bar{x}R_0$ decreases, which can be compensated by more highly connected nodes. Thus, R_0^c increases as population heterogeneity increases, namely as σ_p increases. This is demonstrated for a bimodal network in Fig. 3(a).

Discussion. We have discovered a previously unknown phase transition in the maximum value of the final outbreak size R_{∞}^{\max} , as function of the network heterogeneity strength σ , as R_0 crosses a threshold of R_0^c . While for $R_0 > R_0^c$, R_{∞}^{\max} is obtained at $\sigma = 0$, for $R_0 < R_0^c$, R_{∞}^{\max} is obtained at $\sigma > 0$. This counterintuitive result stems from an intricate balance between the increase in the peak and decrease in the duration

of the epidemic wave, as the network heterogeneity grows. We also showed that population heterogeneity and degree-degree correlations between neighboring nodes strongly affect the value of R_0^c .

What are the implications of this phase transition for realistic scenarios? For diseases such as smallpox, monkeypox, diphtheria, or COVID-19, $R_0 > 2$ is above R_0^c [39–43]. Here, the prediction of the well-mixed SIR model gives an upper bound for R_∞ . Yet, when $R_0 < R_0^c$, taking the well-mixed SIR prediction as an upper bound may be erroneous; e.g., for seasonal influenza ($R_0 = 1.28$ [44]), $\sigma_{\max}/k_0 \simeq 0.857$ for a gamma-distributed network with $k_0 = 20$. This yields $R_\infty \simeq 0.466$, higher by $\sim 16\%$ than the well-mixed prediction $R_\infty \simeq 0.403$. Notably, for positively correlated networks, R_0^c decreases, whereas adding population heterogeneity increases R_0^c . Yet, in Fig. 3(b) we show that the decrease in R_∞^{\max} for all values of σ , due to population heterogeneity, supersedes the increase in R_∞^{\max} due to network heterogeneity. Thus, while evaluating R_0^c and R_∞^{\max} in realistic scenarios is highly nontrivial, these may provide an important insight as to the outcome of the epidemics in the worst-case scenario.

Acknowledgment. A.L. and M.A. acknowledge support from the ISF Grant No. 531/20.

Appendix A: Epidemic threshold for heterogeneous networks. Here we derive the epidemic threshold for heterogeneous networks with degree distribution $p(k)$ as described in the main text. For simplicity we assume the network is uncorrelated, i.e., $\alpha = 0$.

At very early times, the spread of the epidemic is negligible, and the probability that a node remains susceptible, θ , can be approximated as $\theta = 1 - \epsilon$ with $\epsilon \ll 1$, where $\epsilon = \mathcal{O}(k_0^{-1}N^{-1})$ at the epidemic’s initial stage. Using Eq. (3) in the main text, which describes the dynamics of θ , and taking the leading terms in ϵ , yields

$$-\dot{\epsilon} = \left[1 + \frac{R_0}{k_0} - \frac{R_0}{k_0} \frac{\psi''(1)}{\psi'(1)} \right] \epsilon + \mathcal{O}(\epsilon^2). \quad (A1)$$

Using the definition of ψ given by Eq. (2) in the main text, and integrating over time yields

$$\epsilon = \epsilon(0) \exp \left\{ \left[R_0 \left(1 + \frac{\sigma^2}{k_0^2} - \frac{2}{k_0} \right) - 1 \right] t \right\}. \quad (A2)$$

We remind the reader that we are measuring time in units of the inverse recovery rate γ^{-1} . From Eq. (A2), valid at early times, one readily sees that the epidemic spreads as long as the exponent’s argument is positive. As a result, bifurcation occurs when the basic reproduction number satisfies $R_0 = R_0^b$, with

$$R_0^b = \frac{1}{1 + \sigma^2/k_0^2 - 2/k_0} = \frac{k_0^2}{\langle k^2 \rangle - 2k_0}. \quad (A3)$$

As a result, Eq. (A2) can be rewritten as

$$\epsilon = \epsilon(0) e^{(R_0/R_0^b - 1)t}. \quad (A4)$$

These results are consistent with previous results in the large $k_0 \gg 1$ limit [6]. Note that, the typical time scale of the epidemic outbreak, which scales as $1/(R_0/R_0^b - 1)$, diverges as $R_0 \rightarrow R_0^b$. In the well-mixed limit, i.e., $k_0 \gg 1$ and $\sigma \rightarrow 0$, we recover from Eq. (A3) the well-known result of the classical

homogeneous SIR model, $R_0^b = 1$. Yet, for highly heterogeneous networks with $\sigma/k_0 = \mathcal{O}(1)$, R_0^b can be significantly reduced [6].

Appendix B: Network simulations. Here we detail the numerical algorithm used to perform network simulations. In all simulations we have used a Gillespie-based algorithm [34]. In order to create the network of size N with mean degree k_0 and given degree-degree correlation α , for each degree- k node with k initial stems, a fraction α of these stems are connected to other degree- k nodes. The rest are connected to randomly chosen nodes, as in the configuration model, which produces an uncorrelated network [35]. In this way, we obtain a network with correlation α . While the accuracy is high for low values of $\alpha \lesssim 0.3$ (including uncorrelated networks with $\alpha = 0$), as α grows, the accuracy is gradually lost due to finite size effects. Notably, most realistic networks have a correlation parameter of up to ~ 0.3 [36].

Once we have created the network, we run multiple simulations, each starting with an initial number of 100 (out of $N = 10^5$) infected individuals randomly distributed in the network. Within a realization, for each infected-susceptible pair, the rate at which an edge transmits the infection is R_0 in case of a static infection rate, and $\bar{x}(t)R_0$ in case of a dynamic infection rate, see Eq. (10) in the main text. Each infected node can also recover at a rate of $\gamma = 1$. After each infection event, we add the edges which can potentially transmit the infection to the list of transmitting edges, while a recovery event of the base node causes all the edges emanating from it to be removed from the list. The simulation ends when there are no more infected nodes and transmitting edges.

To compute R_0^c , namely to find σ_{\max} for a given R_0 , and the critical basic reproduction number for which σ_{\max} becomes zero for the first time, we performed 1,000 simulations for each value of σ . In order to find σ_{\max} , i.e., the standard deviation which maximizes the final fraction of recovered R_∞ , we used a parabolic fit $ax^2 + bx + c$ (where a is negative) to the dependence of R_∞ on σ , in the vicinity of σ_{\max} . This way, we identified σ_{\max} as the maximum of the parabola, at $-b/(2a)$. Notably, very close to the phase transition there was substantial noise in the results, so we used instead of the parabolic fit, a linear fit to determine whether σ_{\max} was positive or zero.

Appendix C: Comparison between initial and final susceptible degree distributions. Here we study the final degree distribution of susceptible nodes. The initial degree distribution of susceptibles is $p(k)$, as the initial number of infected nodes is negligible. As a result, the probability that a node of rank k is susceptible at time t , $p_s(k, t)$, satisfies

$$p_s(k, t) \simeq \frac{1}{S(t)} p(k) \theta(t)^k. \quad (C1)$$

Here, the probability that an edge has not transmitted the disease is given by $\theta(t) < 1$, see main text, and thus, $\theta(t)^k$ is the probability that none of the edges has transmitted the disease to a degree- k node. Notably, in Eq. (C1), $p(k)\theta(t)^k$ is normalized by $S(t)$, the fraction of the susceptible individuals.

As time evolves, $\theta(t)$ decreases monotonically. Thus, at the final stage of the epidemic the probability to observe high-degree susceptible nodes is very small, while the probability to observe low-degree susceptible nodes remains

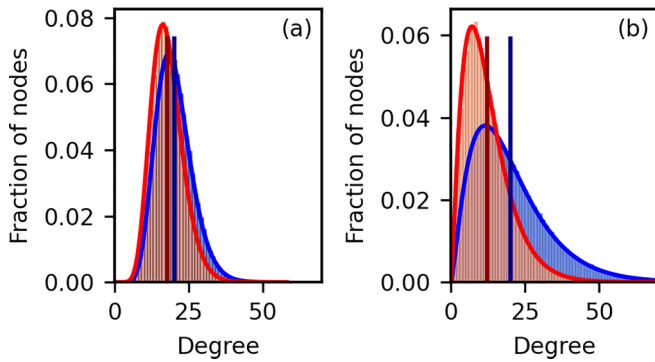


FIG. 4. Degree distribution of susceptible nodes at the initial and final stages of the epidemic. Here, we used a gamma-distributed network with 10^5 nodes, with $k_0 = 20$ and $R_0 = 2$, and averaged over 100 realizations. The blue and red bins represent the degree distribution at the initial epidemic stage ($t = 0$), and final epidemic state ($t = \infty$), respectively. The solid curves represent the theoretical PDF $p_s(k, t)$ [Eq. (C1)], while the vertical lines represent the average value. In panel (a) $\sigma/k_0 = 0.3$, while in panel (b) $\sigma/k_0 = 0.65$.

almost unchanged. This explains why in a population network with high heterogeneity, individuals with more contacts are more likely to get infected early in the epidemic, while

peripheral nodes with a small number of contacts are more likely to remain susceptible at the end of the outbreak. Notably, this effect becomes more dominant as heterogeneity increases, which causes an increase in the relative number of low- and high-degree nodes.

In Fig. 4 we show the initial and final degree distribution of susceptibles. Here, we average over 100 realizations on a gamma-distributed network of size $N = 10^5$ nodes, with $k_0 = 20$ and $R_0 = 2$. One can see that as σ/k_0 increases, the effect becomes more dominant. Here, the vertical lines represent the average of the degree distribution, which shifts to the left as explained above.

We conclude by computing how the mean susceptible's degree $k_s(t)$ changes as the epidemic progresses. At $t = 0$, $k_s(t)$ is very close to k_0 . Thus, using Eq. (C1), the time-dependent mean degree of susceptibles satisfies

$$k_s(t) \simeq \frac{1}{S(t)} \sum_{k=0}^{\infty} k p(k) \theta^k. \quad (\text{C2})$$

For homogeneous networks where $p(k) = \delta_{k,k_0}$, the mean degree of susceptible nodes remains constant $k_s(t) = k_0$, as here, $S(t) = \theta^{k_0}$. In contrast, as heterogeneity increases, the rate of decrease of $k_s(t)$ grows, see Fig. 4.

-
- [1] W. O. Kermack and A. G. McKendrick, A contribution to the mathematical theory of epidemics, *Proc. R. Soc. Lond. A* **115**, 700 (1927).
- [2] R. Anderson and R. May, *Infectious Diseases of Humans: Dynamics and Control* (OUP Oxford, 1992).
- [3] H. W. Hethcote, The mathematics of infectious diseases, *SIAM Rev.* **42**, 599 (2000).
- [4] G. Chowell, L. Sattenspiel, S. Bansal, and C. Viboud, Mathematical models to characterize early epidemic growth: A review, *Phys. Life Rev.* **18**, 66 (2016).
- [5] W. Yang, D. Zhang, L. Peng, C. Zhuge, and L. Hong, Rational evaluation of various epidemic models based on the COVID-19 data of china, *Epidemics* **37**, 100501 (2021).
- [6] R. Pastor-Satorras, C. Castellano, P. Van Mieghem, and A. Vespignani, Epidemic processes in complex networks, *Rev. Mod. Phys.* **87**, 925 (2015).
- [7] M. Saeedian, M. Khalighi, N. Azimi-Tafreshi, G. R. Jafari, and M. Ausloos, Memory effects on epidemic evolution: The susceptible-infected-recovered epidemic model, *Phys. Rev. E* **95**, 022409 (2017).
- [8] M. Bohner, S. Streipert, and D. F. Torres, Exact solution to a dynamic sir model, *Nonlinear Anal. Hybr.* **32**, 228 (2019).
- [9] J. C. Miller, A note on a paper by Erik Volz: SIR dynamics in random networks, *J. Math. Biol.* **62**, 349 (2011).
- [10] E. Volz, SIR dynamics in random networks with heterogeneous connectivity, *J. Math. Biol.* **56**, 293 (2008).
- [11] M. E. J. Newman, Spread of epidemic disease on networks, *Phys. Rev. E* **66**, 016128 (2002).
- [12] E. Kenah and J. M. Robins, Second look at the spread of epidemics on networks, *Phys. Rev. E* **76**, 036113 (2007).
- [13] P.-A. Noël, B. Davoudi, R. C. Brunham, L. J. Dubé, and B. Pourbohloul, Time evolution of epidemic disease on finite and infinite networks, *Phys. Rev. E* **79**, 026101 (2009).
- [14] L. A. Meyers, B. Pourbohloul, M. E. J. Newman, D. M. Skowronski, and R. C. Brunham, Network theory and sars: Predicting outbreak diversity, *J. Theor. Biol.* **232**, 71 (2005).
- [15] F. Ball, A unified approach to the distribution of total size and total area under the trajectory of infectives in epidemic models, *Adv. Appl. Probab.* **18**, 289 (1986).
- [16] F. Ball and D. Clancy, The final size and severity of a generalised stochastic multitype epidemic model, *Adv. Appl. Probab.* **25**, 721 (1993).
- [17] M. Keeling and P. Rohani, *Modeling Infectious Diseases in Humans and Animals* (Princeton University Press, 2008).
- [18] T. House, J. V. Ross, and D. Sirl, How big is an outbreak likely to be? Methods for epidemic final-size calculation, *Proc. Math. Phys. Eng. Sci.* **469**, 20120436 (2013).
- [19] L. J. Allen, A primer on stochastic epidemic models: Formulation, numerical simulation, and analysis, *Infect. Dis. Model.* **2**, 128 (2017).
- [20] J. C. Miller, Distribution of outbreak sizes for SIR disease in finite populations, [arXiv:1907.05138](https://arxiv.org/abs/1907.05138).
- [21] J. Hindes, M. Assaf, and I. B. Schwartz, Outbreak size distribution in stochastic epidemic models, *Phys. Rev. Lett.* **128**, 078301 (2022).
- [22] H. W. Hethcote, An immunization model for a heterogeneous population, *Theor. Popul. Biol.* **14**, 338 (1978).
- [23] N. Becker and P. Yip, Analysis of variations in an infection rate, *Aust. J. Stat.* **31**, 42 (1989).
- [24] A. S. Novozhilov, On the spread of epidemics in a closed heterogeneous population, *Math. Biosci.* **215**, 177 (2008).
- [25] M. G. M. Gomes, M. U. Ferreira, R. M. Corder, J. G. King, C. Souto-Maior, C. Penha-Gonçalves, G. Gonçalves, M. Chikina,

- W. Pegden, and R. Aguas, Individual variation in susceptibility or exposure to SARS-CoV-2 lowers the herd immunity threshold, *J. Theor. Biol.* **540**, 111063 (2022).
- [26] J. O. Lloyd-Smith, S. J. Schreiber, P. E. Kopp, and W. M. Getz, Superspreading and the effect of individual variation on disease emergence, *Nature (London)* **438**, 355 (2005).
- [27] J. Neipel, J. Bauermann, S. Bo, T. Harmon, and F. Jülicher, Power-law population heterogeneity governs epidemic waves, *PLoS ONE* **15**, e0239678 (2020).
- [28] A. V. Tkachenko, S. Maslov, A. Elbanna, G. N. Wong, Z. J. Weiner, and N. Goldenfeld, Time-dependent heterogeneity leads to transient suppression of the COVID-19 epidemic, not herd immunity, *Proc. Natl. Acad. Sci. USA* **118**, e2015972118 (2021).
- [29] M. Assaf and B. Meerson, Extinction of metastable stochastic populations, *Phys. Rev. E* **81**, 021116 (2010).
- [30] M. Assaf and B. Meerson, WKB theory of large deviations in stochastic populations, *J. Phys. A: Math. Theor.* **50**, 263001 (2017).
- [31] Y. Moreno, J. B. Gómez, and A. F. Pacheco, Epidemic incidence in correlated complex networks, *Phys. Rev. E* **68**, 035103(R) (2003).
- [32] Here, we recover the result of random networks for $\alpha = 0$ [45]. Notably, we account for correlations between nearest neighbors only, and neglect long-range correlations. Yet, the model still adequately describes correlated networks [31].
- [33] For $k_0 = \mathcal{O}(1)$ our derivation is invalid since $\epsilon = \mathcal{O}(1)$, and in addition, stochastic effects become dominant, such that R_0^c rapidly grows as k_0 is decreased; see Fig. 1(c).
- [34] D. T. Gillespie, Exact stochastic simulation of coupled chemical reactions, *J. Phys. Chem. C* **81**, 2340 (1977).
- [35] M. Molloy and B. Reed, A critical point for random graphs with a given degree sequence, *Random Struct. Algorithms* **6**, 161 (1995).
- [36] M. E. J. Newman, Assortative mixing in networks, *Phys. Rev. Lett.* **89**, 208701 (2002).
- [37] The maximal relative error in Fig. 2(b) between the numerical and approximated values of R_∞ was $<0.2\%$.
- [38] Naturally, other distributions of susceptibility are possible; yet, these do not qualitatively change our results.
- [39] R. Gani and S. Leach, Transmission potential of smallpox in contemporary populations, *Nature (London)* **414**, 748 (2001).
- [40] R. Grant, L.-B. L. Nguyen, and R. Breban, Modelling human-to-human transmission of monkeypox, *Bull. World Health Organ.* **98**, 638 (2020).
- [41] S. A. Truelove, L. T. Keegan, W. J. Moss, L. H. Chaisson, E. Macher, A. S. Azman, and J. Lessler, Clinical and epidemiological aspects of diphtheria: A systematic review and pooled analysis, *Clin. Infect. Dis.* **71**, 89 (2020).
- [42] M. A. Billah, M. M. Miah, and M. N. Khan, Reproductive number of coronavirus: A systematic review and meta-analysis based on global level evidence, *PLOS ONE* **15**, e0242128 (2020).
- [43] Y. Liu and J. Rocklöv, The effective reproductive number of the omicron variant of SARS-CoV-2 is several times relative to delta, *J. Travel Med.* **29**, taac037 (2022).
- [44] M. Biggerstaff, S. Cauchemez, C. Reed, M. Gambhir, and L. Finelli, Estimates of the reproduction number for seasonal, pandemic, and zoonotic influenza: a systematic review of the literature, *BMC Infectious Diseases* **14**, 480 (2014).
- [45] S. L. Feld, Why your friends have more friends than you do, *Am. J. Sociol.* **96**, 1464 (1991).